Study of Honeycomb Strip Chamber Preradiator for KOPIO

G.S. Atoyan, V.V. Issakov, A.A. Poblaguev, and M.E. Zeller
Physics Department, Yale University, New Haven, CT 06511

O.V. Karavichev and T.L. Karavicheva
Institute for Nuclear Research of Russian Academy of Siences, Moscow 117312, Russia

November 3, 2000

Abstract

Prototypes of Honeycomb Strip Chambers have been designed and constructed for a preradiator for the KOPIO experiment. Chambers have been tested with cosmic ray muons, and a set of six were studied in a low energy $(100 \div 300)$ MeV photon beam. Construction details and test results of spatial and angular resolution are presented.

1 Introduction.

The requirements of the preradiator for KOPIO experiment [1] include a photon angular resolution of approximately 25 $mrad$, a photon conversion efficiency of about 0.7 $(2.0X_0)$, a good measurement of the deposited energy and as short as possible linear extent so as to limit shower size at the calorimeter. One of the possible designs for a preradiator element is considered in the Proposal as a "Honeycomb Strip Chamber" (HSC) with integrated scintillator. Six planes of prototypes of an HSC with sensitive area 33×33 cm^2 have been constructed and tested using cosmic ray muons and a photon beam obtained at the BNL NLSC.

2 The chamber design

The design principle of the HSC is shown on Fig. 1. Each anode wire is coaxially surrounded by a conducting cathode which is effectively a hexagonal tube. The half of this tube is a directly grounded conductive layer (shown in grey) and other half is formed by a set of corrugated strips virtually grounded via amplifiers. This structure forms two layers of hexagonal drift tubes with a common layer of the strip readout. A strip-ground capacity is small since a gap between the edges of grounded layers and strips is about 1 mm. The anode wires are individually connected to a positive HV supply via 10 M Ohm resistors.

Our prototype preradiator chamber is based on the described design principle with integrated scintillators illustrated in Fig. 2. The drift tubes are formed by corrugated, polyamide/copper laminated foil and metallized scintillators, which provide mechanical strength to total structure. In the honeycomb arrangement, when the three pieces shown in Fig. 2 are joined, two close packed rows of hexagonal drift tubes are formed. The cell size of each tube is 7.9 mm between parallel faces. The central foil has strips on both sides, which are electrically connected. An attractive feature of this chamber arrangement is the nearly cylindrical geometry in which the strips cover half the circumference of the tubes thus subtending half the induced charge. Where the scintillators make contact with the strip foil they are not metallized; otherwise they are metallized and contacted to ground.

As an integral component of the tubes, the scintillators of the prototype chambers have been constructed precisely from sheets of the standard plastic scintillator (BC408) by machining. The scintillator side facing the tubes has been formed to the corrugated shape of the tubes. The opposite side contains grooves every 13.68 mm, into which have been placed the wavelength shifting (WLS) fibers for reading out the scintillator light. The cross section of grooves is $1.1 \times 1.1\ mm^2$. The diameter of Kuraray WLS fiber is 1 mm. For a metallization of the scintillator we have used a silver-filled acrylic paint with a conductivity of 0.1 ohm/square. Before metallization the scintillators were covered with a reflective layer of white paint and then a light-isolated layer of black paint.

The middle strip electrode is made from special polyamide/copper laminated foil with the soft polyamide film having thickness of 30 μm and with total two copper layers being 70 μm thick. In this manner only the copper layers define the mechanical strength of corrugated foil structure. The strip

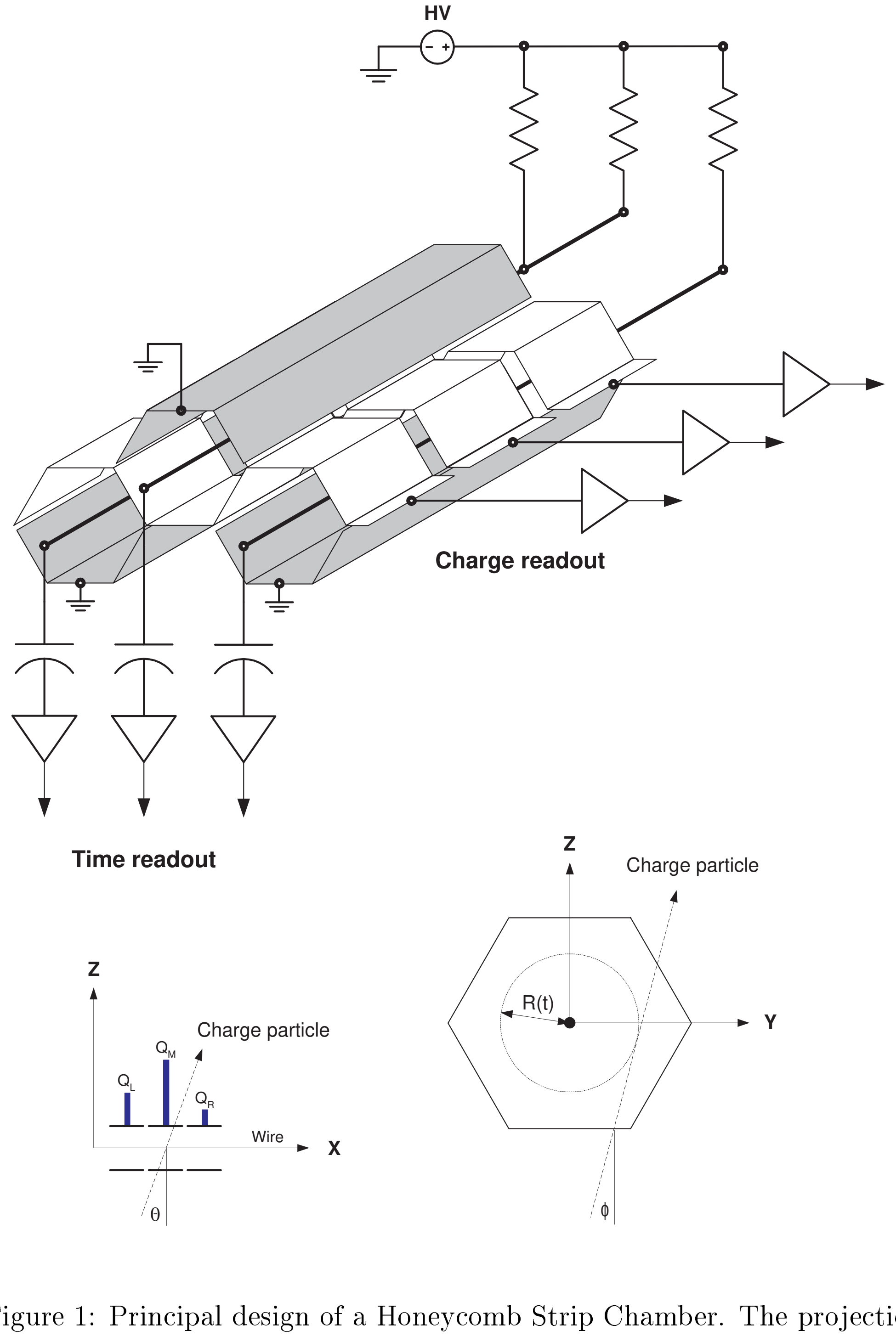

Figure 1: Principal design of a Honeycomb Strip Chamber. The projections orthogonal to wires and to strips are displayed.

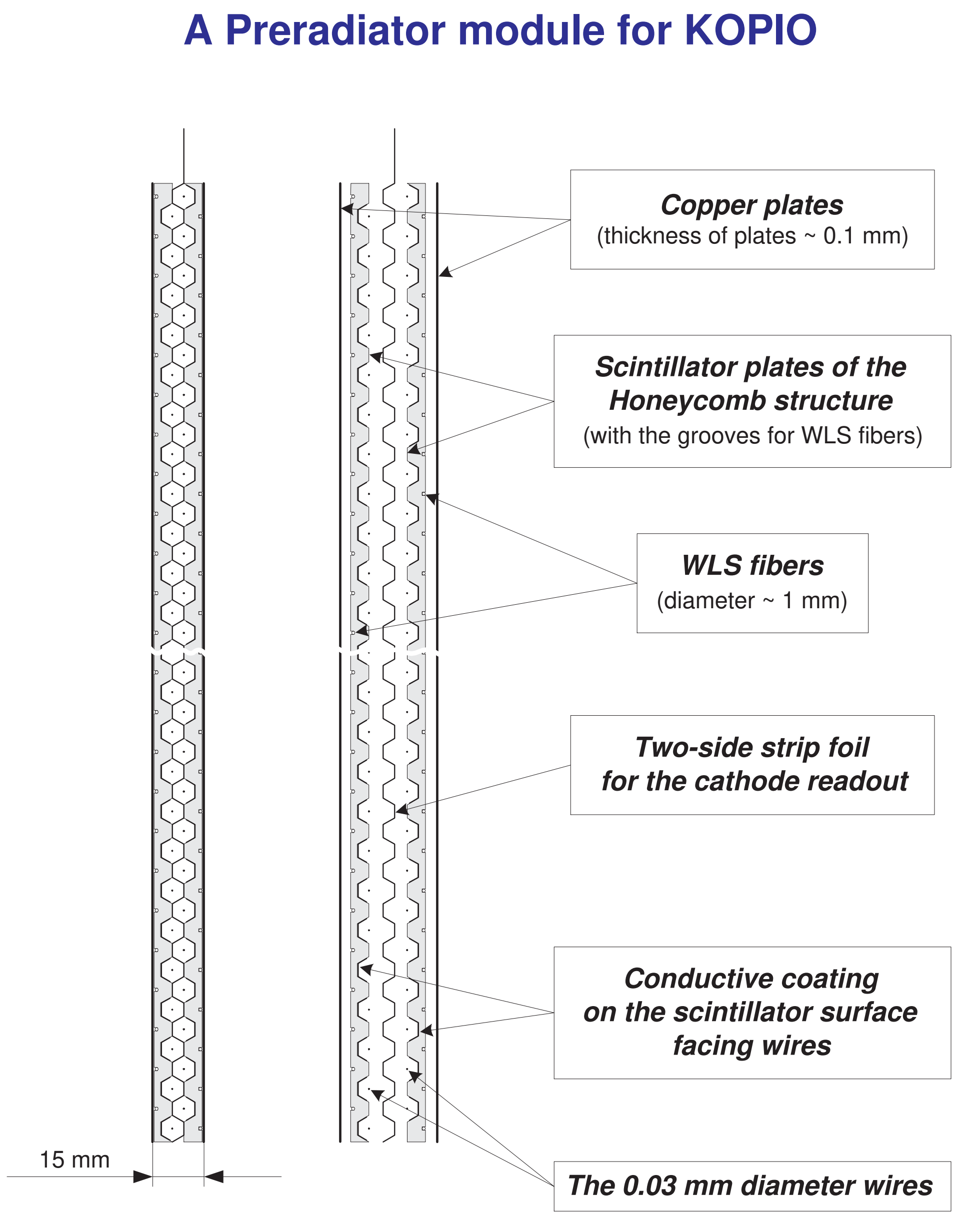

Figure 2: End view of HSC prototype.

Characteristics of HSC	Value
Wires per plane	48
Strips per plane	48
Inner cell diameter (mm)	7.9
Wire length (m)	0.40
Wire diameter (μm)	30
Wire pitch (mm)	6.84
Strip length (m)	0.40
Strip width (mm)	5.84
Strip pitch (mm)	6.84
Folded strip foil:	
thickness of copper/polyamide/copper (μm)	35/30/35
Scintillator thickness (flat to flat) (mm)	5.5
Effective thickness of two scintillator layers (mm)	7.0
WLS fiber per plane	24
Fiber diameter (mm)	1.0
Thickness of two plate of copper converters (mm)	0.2
Total radiation length of chamber (X_0)	0.036

Table 1: Characteristics of the HSC prototypes.

pattern is etched by the standard flexible printed board technology. A precision better than 0.1 mm on the position of strip edges was guaranteed. The foil with flat dimension of $350 \times 500\ mm^2$ was folded by means of specially produced templates. Assembly of the chambers was also accomplished with special templates. The completed chambers were fixed onto an aluminum base plate supported by a stand which allowed the stack of six chambers to be rotated over horizontal angles. The characteristics of the prototype chambers are shown in the Table 1.

3 Operating gas and HV

There are four basic requirements that need to be met by a chamber gas suitable for HSC:

- High drift velocity ($> 50\mu$m/ns)
- Composition stability of gas mixture

- Temperature stability
- Non-flammable
- Low cost.

For our first stage of the R&D of the preradiator HSC chambers we have chosen an inexpensive commercial $P10$ – mixture: 90%Ar + 10% methane. During longtime "cosmic ray" measurements we found a very high stability of gas parameters (gain, drift velocity) of this mixture and never observed high voltage break down effects.

Positive HV was applied to the wires. Its value was chosen as a compromise between the following requirements:

- Effective use of the ADC range,
- Discriminator threshold of 10 mV,
- Optimization of noise/signal ratio,
- Gas gain of $(2-5)\times 10^5$ for both good spatial resolution of the cathode strip readout and good efficiency of the wire readout.

The chosen value of HV was 1500 V ($\pm$20 V for individual HSCs) which corresponded to a gas gain of about 4×10^5.

4 Electronics and DAQ system

The readout chains of both wires and strips are schematically shown on Fig. 1. The current signals on the wires are amplified as close to the chamber as possible. The amplification and discrimination of signal is done with a fast (rise time ~ 7 ns) 16-channel amplifier-shaper constructed at INR (Moscow) for proportional chambers. The linear amplifier is based on a fast transistor, KT316, and 1/4 of a MC10125 integrated circuit. The discriminator with variable threshold setting is realized by using a fast comparator, AM685. The range of the threshold was $7 \div 50$ mV. The overall gain of the preamplifier and amplifier provides a charge sensitivity of 10 V/pC e.g. a threshold signal of 10^4 electrons produces 15 mV at the input of the comparator. The time shaping of the signal is provided by RC-chain. Output signals with variable width setting ($20 \div 100$ ns) are ECL levels. These bipolar signals are transported by twisted pair cables of approximately 40 m length to the 96- channel LeCroy 1877 TDC (FASTBUS standard) with a binning of 0.5 ns.

For the strip readout we have used a modernized AMPLEX system [2]. It is a compact, low cost readout system with small number of cables.

This CMOS integrated circuit system was designed at CERN for use with silicon detector with small (< 10 pF) capacitance. The AMPLEX chip contains 16 channels, each consisting of a charge amplifier, a shaper amplifier with semi-gaussian shaping form and track-and-hold stage with storage capacitors, analog multiplexer and a unity gain buffer output amplifier. The analog multiplexer is controlled by digital circuitry. Peaking time of system may be adjusted in $400 \div 800$ ns range. To obtain adequate noise performance with cathode readout chamber a hybrid charge sensitive preamplifier was included in front of each AMPLEX channel [2]. This preamplifier has JFET front end optimized for an input electrode capacitance range of $50 \div 150$ pF. the cathode strip capacitance of our HSC prototype (~ 50 pF).

A total of 4096 channels may be read by single CAMAC module, which digitizes the analog signals with a 10-bit flash ADC and stores the information in a memory. For our test measurements we have used a 3-board AMPLEX system (each 64 channels) coupled to strips by short (~ 20 cm) flat cables. The chosen peaking time was 400 ns.

For FASTBUS readout we used an STR340 VME to FASTBUS interface (SFI). The SFI was controlled by an MVME 2305 Power PC - based single board computer running VxWorks, The data were transferred to the host PC over ethernet. For CAMAC readout we used the STR320 FASTBUS to CAMAC interface. The DAQ software running on the MVME 2305 and on the host PC were originally developed for the BRAHMS experiment at RHIC [3, 4].

5 Calibration of HSC

5.1 Charge calibration

The GEANT simulations show that cathode strip gains should be calibrated with relative accuracy of $< 2\%$ to achieve a good spatial resolution resolution ~ 100 μm. Two calibration procedures have been tested.

Precision calibration capacitors of 0.2 pF were built into the readout board of AMPLEX system and connected to each strip channel. A precision pulser was fed to the all calibration capacitors, where the amplitude of this pulser as well as its trigger was computer controlled. Calibration data were taken by stepping the pulser amplitude through 30 values covering the total dynamic range of ADC. Several hundred events were accumulated for every pulser amplitude. A polynomial fit of these data was used to calculate relation $Q(amp)$ between the induced charge and the signal amplitude.

The calibration procedure was checked with cosmic ray muons. The strip ADC channels were calibrated to minimize the χ^2 of reconstructed muon tracks.

The two calibration methods coincided with each other with an accuracy of about 1%. This indicates that the pulser calibration is adequate for the requirement spatial resolution. This calibration method is easy to implement, needs no spatially uniform particle beam and is less time than consuming than calibration based on the fits to the muon tracks.

Pulser calibration were performed once per run during the test measurements.

5.2 Drift time calibration

Calibration of the dependence of the distance between anode wires and particle tracks on drift time, $R(t)$, is important in obtaining good spatial resolution in the wire readout analysis. Since we had no precise coordinate detectors for direct measurement of $R(t)$ dependence, the following calibration procedure was applied:

The HSC was uniformly exposed by cosmic ray muons. The distribution density of measured drift time $r(t)$ may be converted to $R(t)$ as

$$R(t) = \alpha \int_{t_0}^{t} r(\tau) d\tau + \beta$$

Here, t_0 is minimal drift time, corresponding to the particle passing through the wire, and α and β are adjustable parameters. α defines the coordinate scale and β corrects uncertainties in t_0. Actual values of α and β were determined by minimization of χ^2 for reconstructed muon tracks. Fig. 3–5 illustrates the process of calibration of the drift time.

6 Data analysis

6.1 The wire data analysis

Track finding in wire data analysis was performed as follows:

- Planes with "good" signals were selected. "Good" means only one or two consequent wires hits per plane. Only hits with times corresponding acceptable radius $0 < R < R_{tube}$ were taken into account.
- The best track was found using all selected planes. This step included the resolving of the "left-right symmetry" for all hits.
- All or only few selected coordinates were used to define track parameters. In case of low energy photons (e^+e^--pair) the selected coordinates from only first 2-3 planes were used to reduce effects of multiple scattering.

6.2 The strip data analysis

The track finding in cathode strips is much simpler because there is no "right-left symmetry" problem and the effect of splitting of e^+e^--pairs is suppressed. The following steps were performed to find tracks in cathode strips:

- The amplitude of each strip was corrected for the particular channel gain calibration.
- The cathode strip planes with a "good" strip clumps were selected. A "good" strip clump is a group of the consequent strips about the one maximum.
- The track coordinates are calculated for the selected cathode strip planes. Two algorithms were used: *(i)* three node center of gravity coordinate with a systematic shift correction and *(ii)* Gaussian fit of three strips of the clump. According to Monte Carlo calculations, both algorithms give roughly the same spatial resolution, but the latter method is less sensitive to calibration uncertainties and noise contributions.
- A linear fit was applied to all or only few selected coordinates to determine the track parameters.

7 Detector performance

Cosmic ray data was used to study the spatial resolution the HSCs and for electronic calibration and tuning the algorithms for off-line analysis. Study of photon angular resolution was performed with $100 \div 300$ MeV photon beam for three values of incident angle θ: $\theta = 0°,\ 15°,\ 30°$. In these measurements the incident angle ϕ did not change from $\phi = 0°$.

7.1 Cosmic ray muons measurements

The three first generation HSC chambers were tested in a cosmic ray setup with geometric acceptance optimized for vertical muons. The size and position of two trigger scintillators limited the measured angle to 0.45 rad in all directions. A cutoff muon energy of ~ 0.3 GeV was achieved with 15 cm of lead, located between the HSC detector and the lower trigger scintillator.

Some important characteristics describing the response of HSC prototypes to cosmic rays are displayed on Fig. 6 – 9. The reconstructed coordinate and angular profiles of the detected cosmic rays are presented on the Fig. 10–13. Fig. 14 shows the measured residual resolution of strip readout planes for the total angular range of detected particles. The measured distribution exhibits significant tails which indicate a strong dependence of the spatial resolution on the incident angle of the particle trajectory. This dependence is shown on the Fig. 15. It is approximately a linear function of the incidence angle over the full angular range. Our data on the θ dependence agree well with a theoretical parameterization [6] and with a experimental results from [7]. Spatial resolution is practically insensitive to the ϕ angle. The extrapolated spatial resolution of the HSC strip readout is $\sigma_x = 83\ \mu$m at $\theta = 0°$

The measured residual resolution of the wire readout HSC planes for the total angular range of detected cosmic ray muons is shown in Fig. 16. The distribution is described by a two Gaussian fit with $\sigma_y = 77\mu$m and 220 μm.

7.2 Photon beam measurements

The stack of HSC prototypes were tested at the X5 gamma beam at BNL NSLC. All of the runs used an untargeted photon beam with an energy range of 50 - 400 MeV and intensity of $\sim 10^6$ sec^{-1}. Beam divergence was limited to 2 mrad. The beam had an approximately 2 cm diameter cross section at the location of the detector.

The detector included the six-layers HSC modules, a nonet of Shashlik style calorimeter modules and two trigger scintillators. The Shashlik modules were located downstream of the preradiators. One trigger scintillator (veto) was located upstream of the entire configuration and another (coincidence) between the calorimeter and the chambers. The whole detector was packaged compactly and was installed on a horizontally rotating table which allowed θ angle variation. Anode wires were horizontally and cathode strips were vertically oriented. A trigger signal is formed by a coincidence between the Shashlik calorimeter (cutoff energy of $\sim$ 20 MeV) and the coincidence scintillator, and no signal in the veto scintillator. For the special calibration run with the horizontal cosmic ray muons the veto requirement was removed. The muon runs were used for absolute energy calibration of the calorimeter and for computation of $R(t)$ for the HSC wires.

Fig. 17 shows the measured energy spread of the photon beam as seen by the Shashlik calorimeter. The absolute normalization of the energy scale was made by comparison of GEANT simulated muon signals and the measured signals from the cosmic ray calibration runs. The precision of this normalization is $\sim$ 10%. The measured distribution of the number of hit calorimeter modules per photon clump, *i.e.*, the size of photon clumps, is shown in the same figure. The measured size of the photon beam at the second HSC is shown in Fig. 18, and examples of photon signals in the preradiator modules are displayed on Fig. 19.

100,000 trigger events at the each incidence angle orientation ($\theta = 0°$, $15°$, $30°$; $\phi = 0°$) were used for analysis of reconstructed photons. A total of 11,000 events with a conversion vertex at the second HSC has been selected out of each 100,000-trigger event set. This primary selection included following cuts: photon energy within a $100 \div 300$ MeV range, no signal at first HSC, one "good" wire hit and one "good" strip clump at second HSC, signals in at least two additional HSC planes. The reconstruction algorithm accepted photons with single "good" wire hit (strip clump) and at least in three HSC planes, and rejected a multi-hit events and events with a splitting e^+e^--pairs. The total amounts of these events are $(2.3 - 3.0)\%$ (strip readout) and $(4.2 - 5.1)\%$ (wire readout) and define the inefficiency of photon track finding. Results of the selection and reconstruction procedure are presented at Table 2. As seen from this Table, the recognition efficiency of this simple algorithm is very high - around 95% for both cathode strip and anode wire readout. Some difference of efficiencies between the strip readout and wire readout can be explained by the lack of refinement of the wire algorithm

Cuts	Photon beam $\theta = 0°$ $\phi = 0°$	Photon beam $\theta = 15°$ $\phi = 0°$	Photon beam $\theta = 30°$ $\phi = 0°$
Cathode plane			
$N_{plane\ with\ a\ single\ \text{``}good\text{''}\ strip\ clump} > 2$	97.7%	97.8%	97.0%
$N_{plane\ with\ a\ single\ \text{``}good\text{''}\ strip\ clump} > 2$ $Q_{hit} < 1024$	95.2%	95.3%	95.0%
Wires			
$N_{plane\ with\ a\ single\ \text{``}good\text{''}\ wire\ hit} > 2$	95.8%	95.5%	94.9%
$N_{plane\ with\ a\ single\ \text{``}good\text{''}\ wire\ hit} > 2$ $\chi^2_{best\ left-right\ combination} < 10$	93.0%	93.1%	92.7%

Table 2: Efficiencies of photon track reconstruction. Efficiencies were calculated for sample of 11 thousand photons in the energy range of $100 - 300$ MeV, with no hits in first plane and one and only one "good" both wire hit and strip clump.

for two-track patterns, and by insufficient precision in calculating the R(t) relations.

Some important characteristics, describing the response of HSC preradiator to photons are presented in the Fig. 20–23.

The measured angular distributions of detected photons are shown in Fig 24–26. Track directions have been calculated using only two first selected planes for strip readout and only the first three planes in a track for the wire readout. The angular resolution (gaussian fit) is presented in Table 3.

8 Conclusion

Test measurements of the prototype of honeycomb strip chamber using cosmic rays muons indicate a ~ 150 μm spatial resolution both for wire and strip readouts. Test measurements with 6 layers of HSC performed in a photon beam yielded a photon angular resolution of about 25 mrad ($E_\gamma = 250$ MeV and $\theta = 0°$) for strip readout, consistent with GEANT simulations.

For the wire readout the angular resolution was ~ 32 mrad for $E_\gamma = 250$ MeV. A possible explanation for the difference between the wire and strip resolutions is the absence of a satisfactory drift time calibration during the

	Photon beam $\theta = 0^\circ$ $\phi = 0^\circ$	Photon beam $\theta = 15^\circ$ $\phi = 0^\circ$	Photon beam $\theta = 30^\circ$ $\phi = 0^\circ$
Strip readout			
$100 - 200$ MeV	$\sigma_\theta = 31$ mrad	$\sigma_\theta = 35$ mrad	$\sigma_\theta = 44$ mrad
$200 - 300$ MeV	$\sigma_\theta = 25$ mrad	$\sigma_\theta = 31$ mrad	$\sigma_\theta = 41$ mrad
Wire readout			
$100 - 200$ MeV	$\sigma_\phi = 37$ mrad	$\sigma_\phi = 37$ mrad	$\sigma_\phi = 37$ mrad
$200 - 300$ MeV	$\sigma_\phi = 32$ mrad	$\sigma_\phi = 33$ mrad	$\sigma_\phi = 34$ mrad

Table 3: The angular resolution of HSC preradiator prototype.

photon beam measurements. It is anticipated that in the KOPIO experiment the $x-y$ orientation of ajacent planes will be alternated. In this configuration wire calibration can be achieved with strips from ajacent chambers. This alternation of chamber orientation will also improve the resolution of the "left-right symmetry" in drift time coordinates when the particle trajectories pass through only one cell.

That the angular and spatial resolutions of the prototype HSC system agree with those of our GEANT calculations give us confidence that a preradiator for the KOPIO experiment can be constructed which will meet the required specifications for the experiment. The next stage of development of these devices is construction and testing of fullscale (2m by 2m) prototypes.

Acknowledgements

We gratefully acknowledge the contributions to the success of photon beam measurements by A. Sandorfi, S. Hoblit, L. Miceli, C. Thorn of NP/LEGS who provide us the possibility of these measurements.

We are indebted to K. Olchanski for help in maintaince and operating DAQ System.

References

[1] KOPIO Proposal, http://sitka.triumf.ca/e926/

[2] G.Bencze *et. al.*, NIM A357 (1995) 40.

[3] K. Olchanski, private communication

[4] http://pii3.brahms.bnl.gov/∼daq/oncs/doc/

[5] Hoite Tolsma, *The Honeycomb Strip Chamber: A two coordinate and high precision muon detector*, NIKHEF PhD Thesis, Amsterdam, 1996; http://atlasinfo.cern.ch/Atlas/documentation/thesis/nikhef/tolsma.ps.gz

[6] P. Rehak and E. Gatti, *Semiconductor Detectors in Nuclear and Particle Physics*, Proceedings of the 5th Conference on the Intersections of Particle and Nuclear Physics, p. 195, 1994, St. Petersburg, Florida, USA

[7] Harry van der Graaf *et. al.*, NIM A307 (1991) 220.

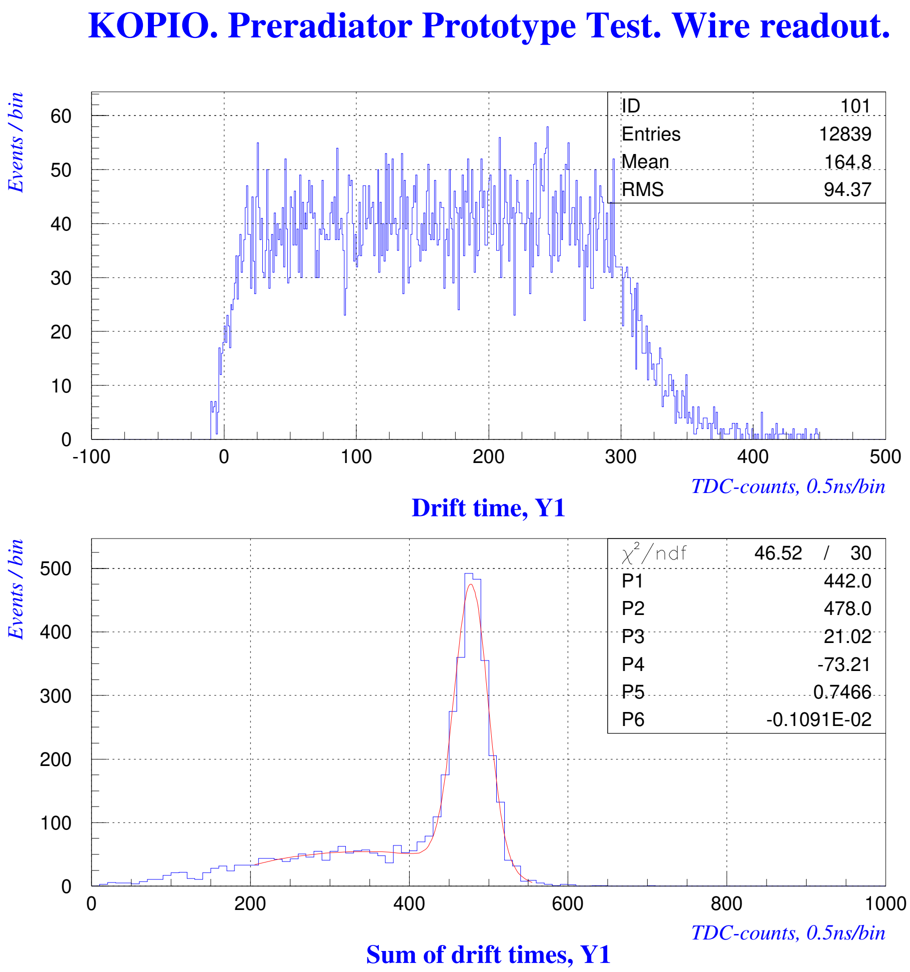

Figure 3: The typical distribution of the measured TDC values for one HSC cell (top) and the typical distribution of the sum of measured TDC values for two neighboring cells (bottom). HSC detector is exposed by cosmic ray muons.

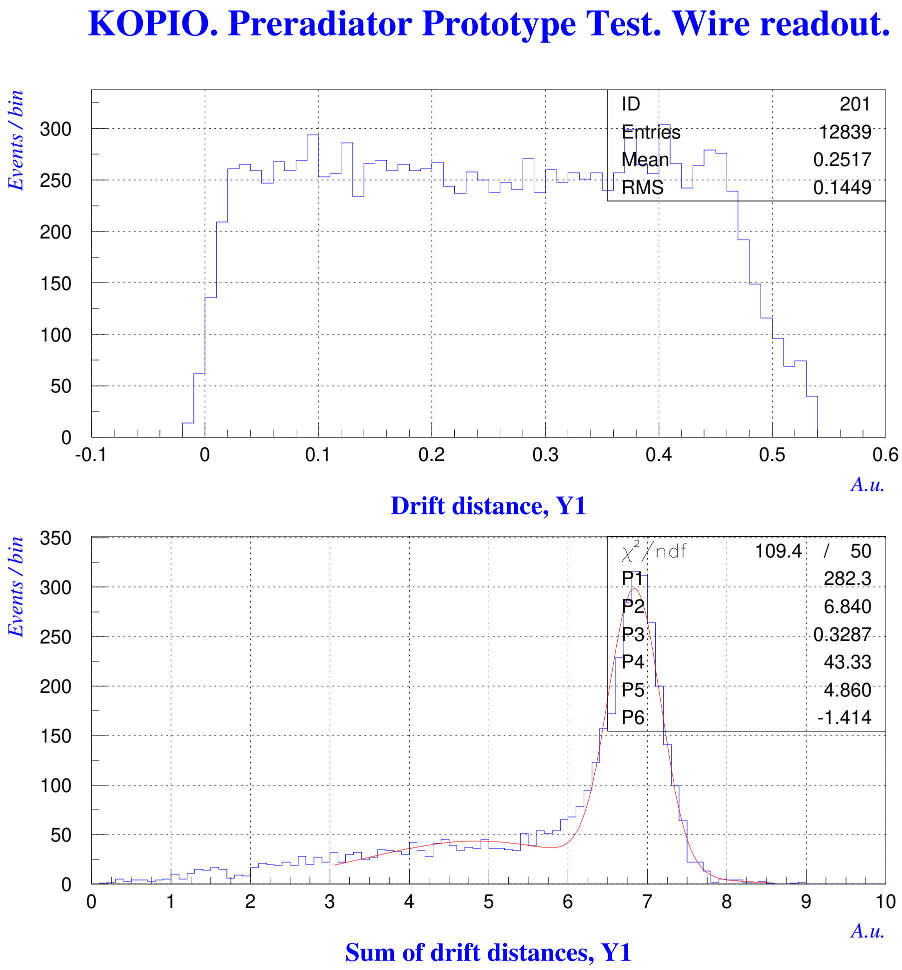

Figure 4: The typical distribution of the reconstructed drift distance values for a one HSC cell (top) and the typical distribution of the sum of reconstructed drift distance values for two neighboring cells (bottom) for muons. The value of 0.5 on the top histogram is consistent with the inner radius of a cell. The value of 6.84 cm on the bottom histogram is consistent with the wire pitch.

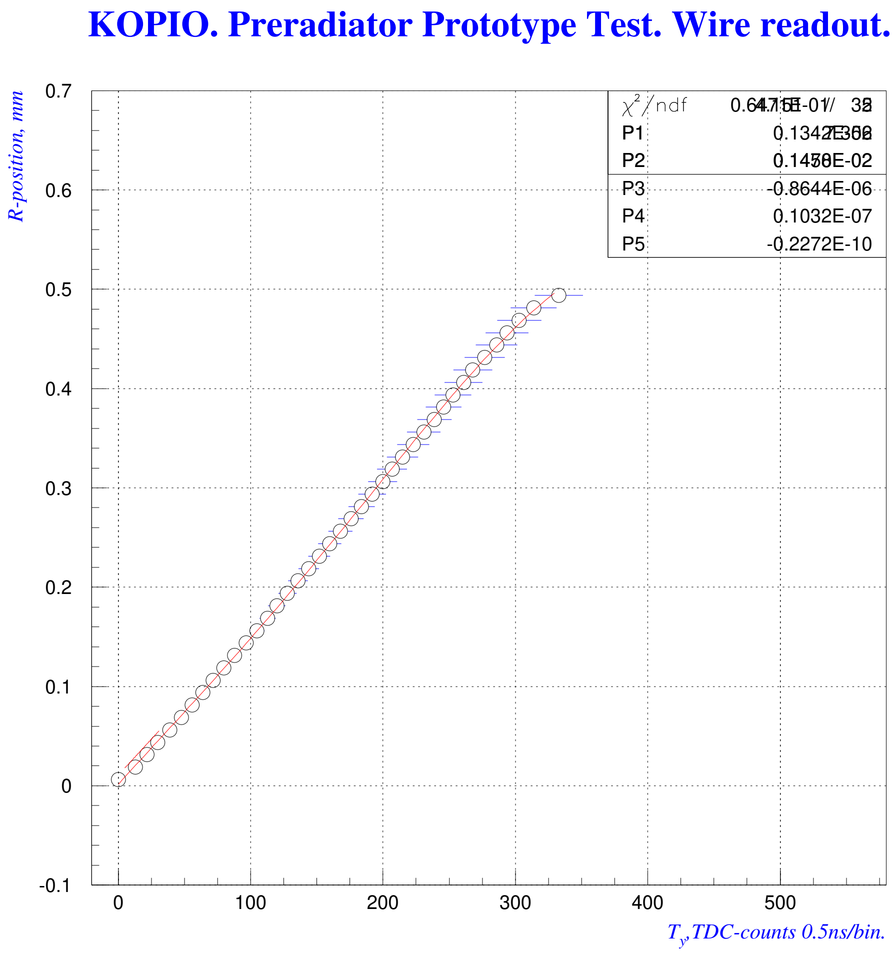

Figure 5: R(t) vs. TDC counts as computed assuming that the distribution of muons is uniform across a cell.

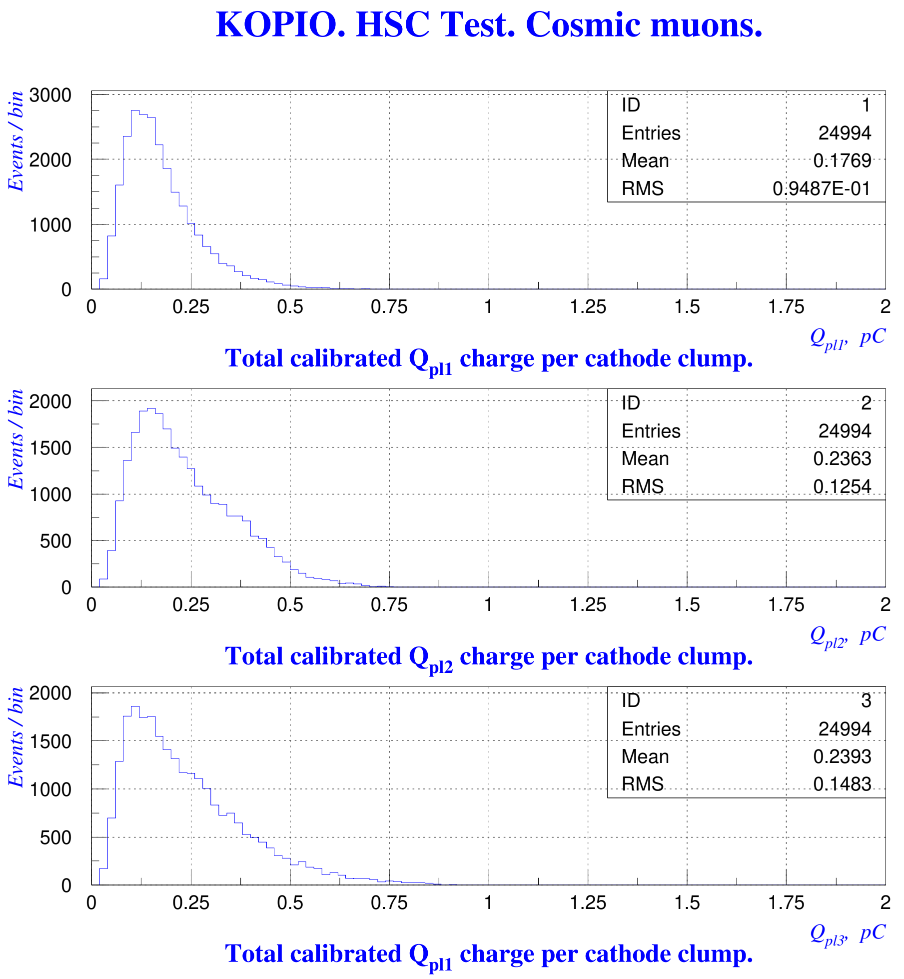

Figure 6: Observed collected charge distribution for incident cosmic ray muons.

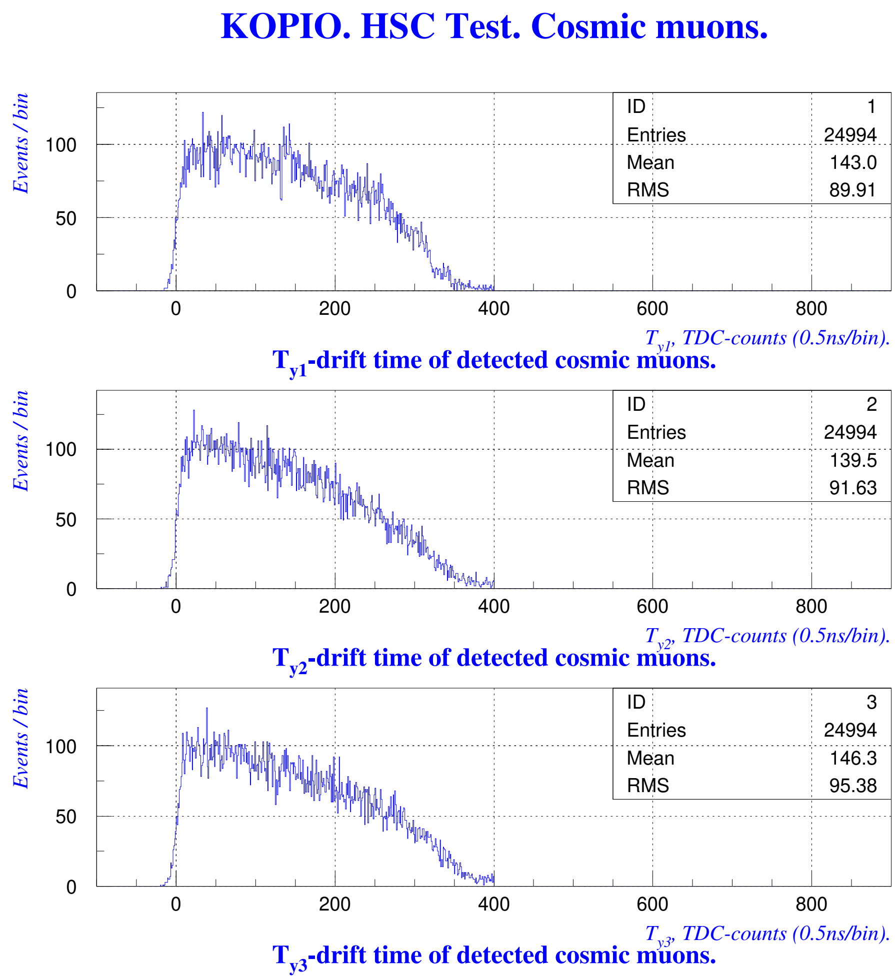

Figure 7: Drift time distribution of cosmic ray muons.

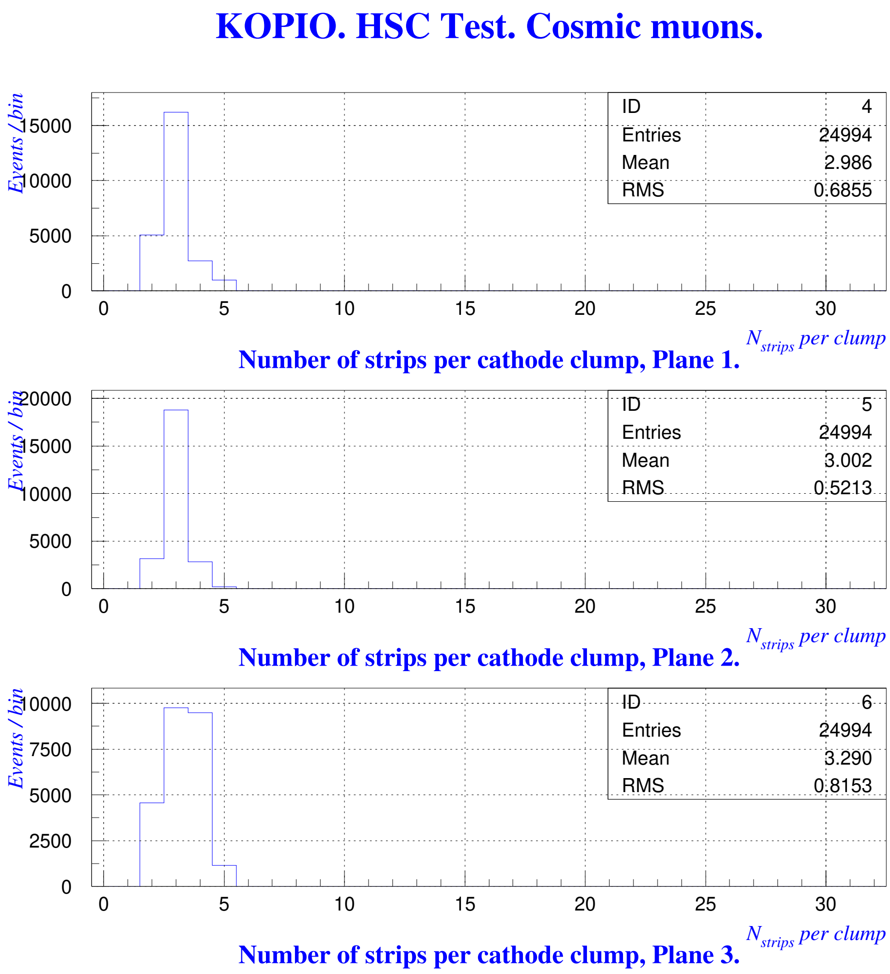

Figure 8: Number of strips per cosmic ray muon event for three chambers.

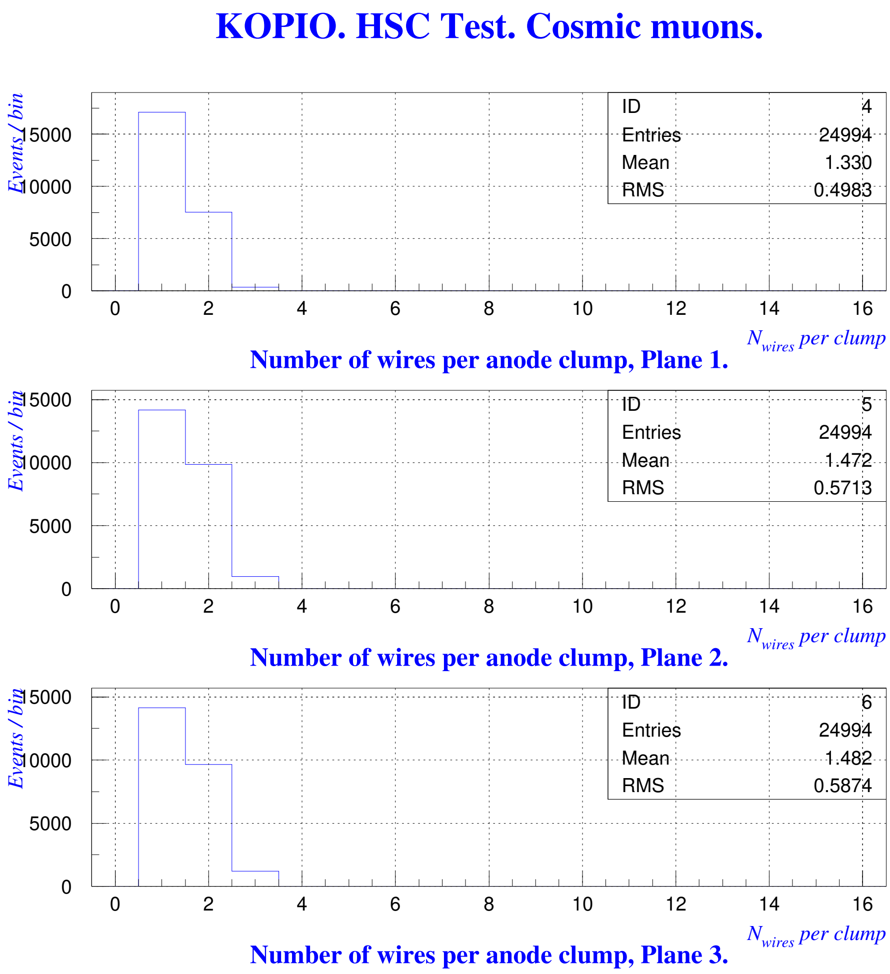

Figure 9: Number of wires per cosmic ray muon event for three chambers.

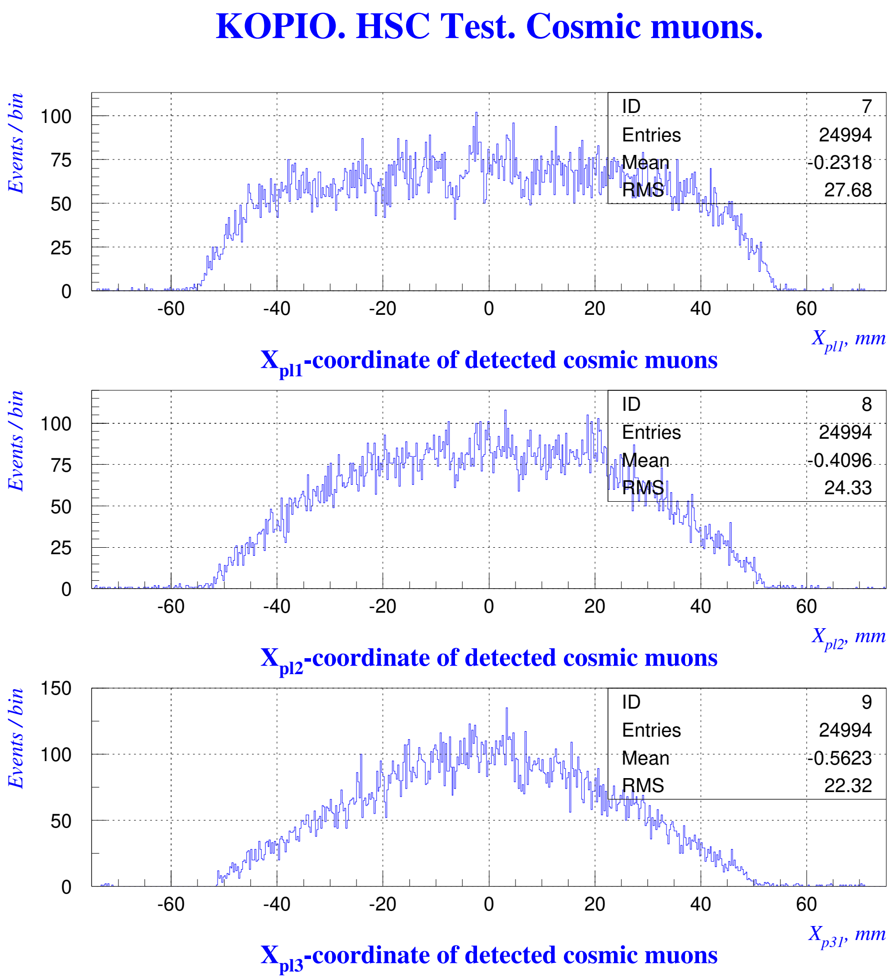

Figure 10: Coordinate profile distribution for reconstructed cosmic ray muons tracks using strips.

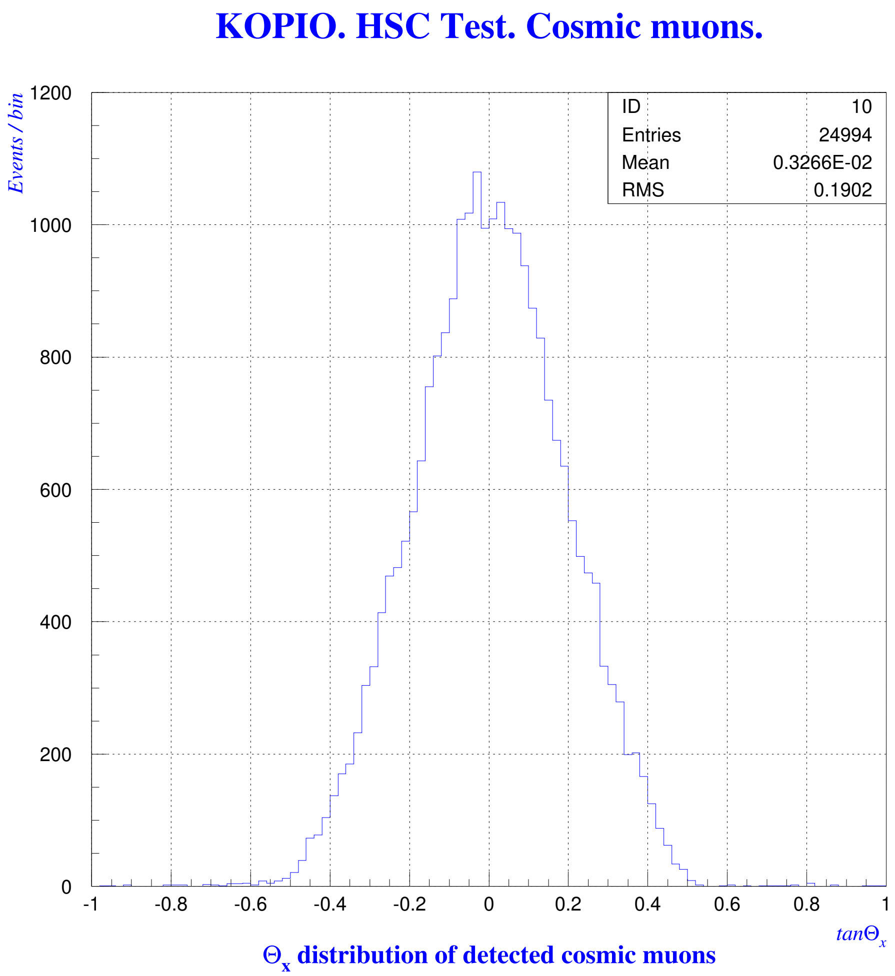

Figure 11: Angular profile distribution for reconstructed cosmic ray muons using strips.

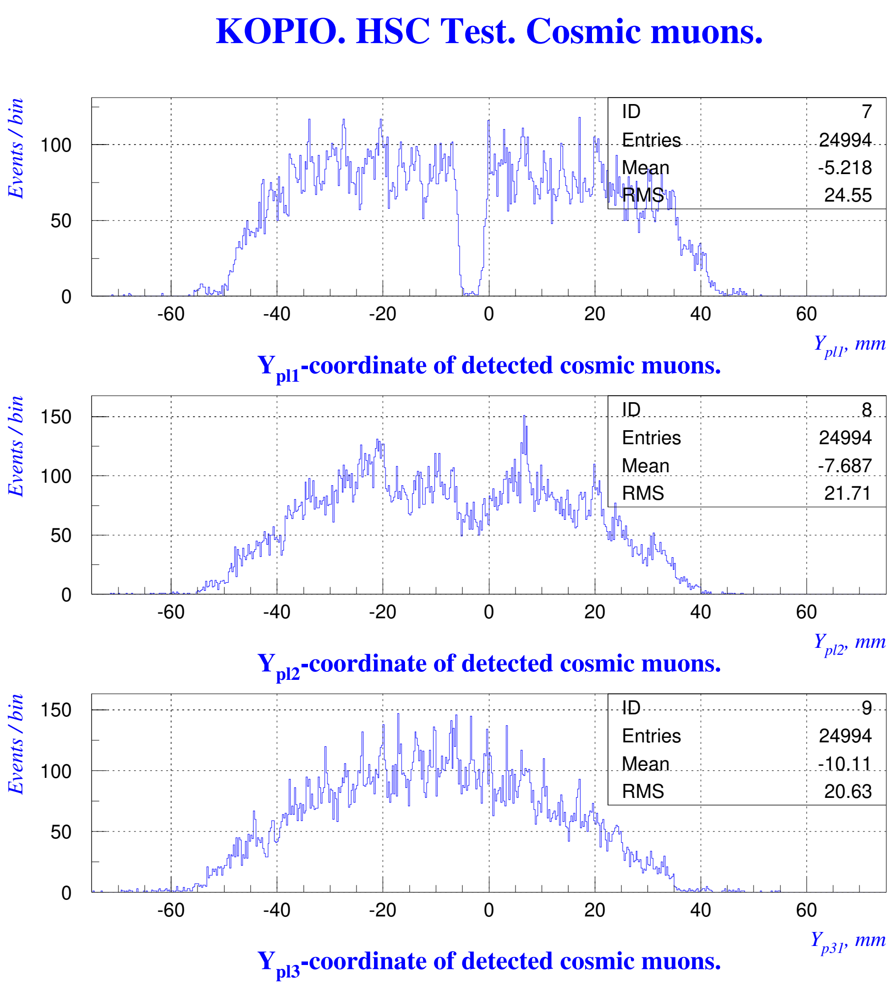

Figure 12: Coordinate profile distribution for reconstructed cosmic ray muons using wires.

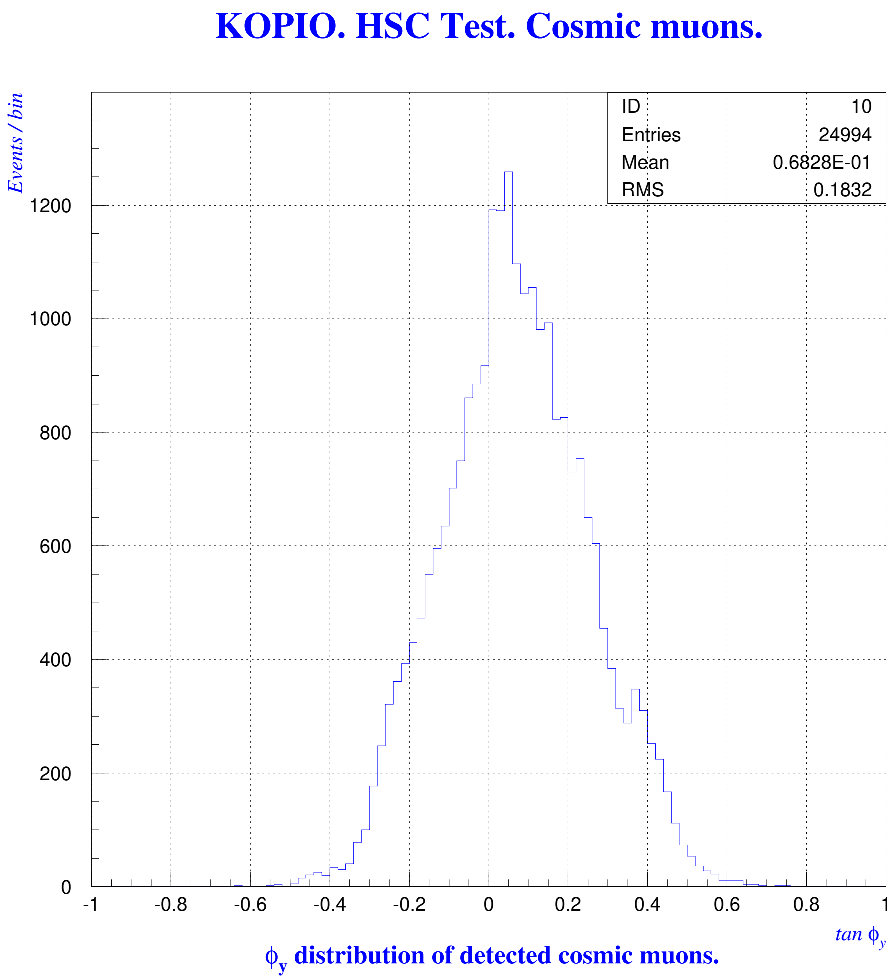

Figure 13: Angular profile distribution for the reconstructed cosmic ray muons using wires.

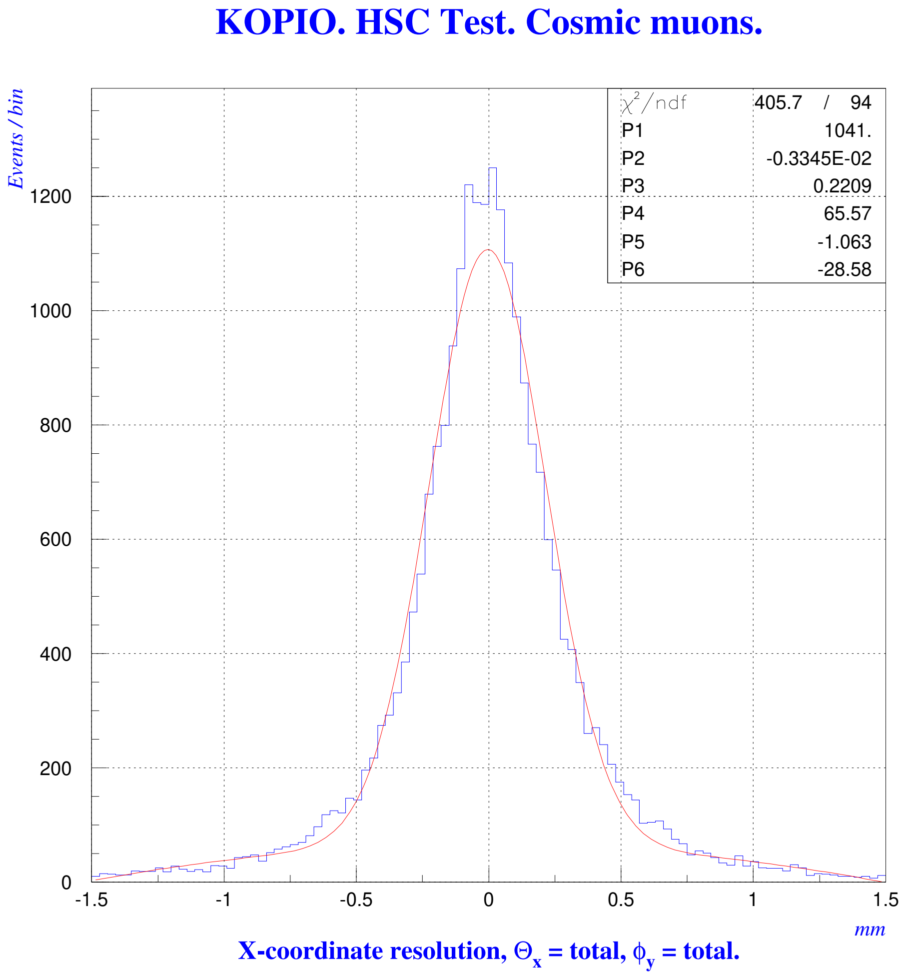

Figure 14: The measured residual resolution of strip readout planes for the total angular range of the detected cosmic ray muons. The solid curve is the sum of a Gaussian plus polynomial fit. The Gaussian fit has $\sigma_x = 220\ \mu m$.

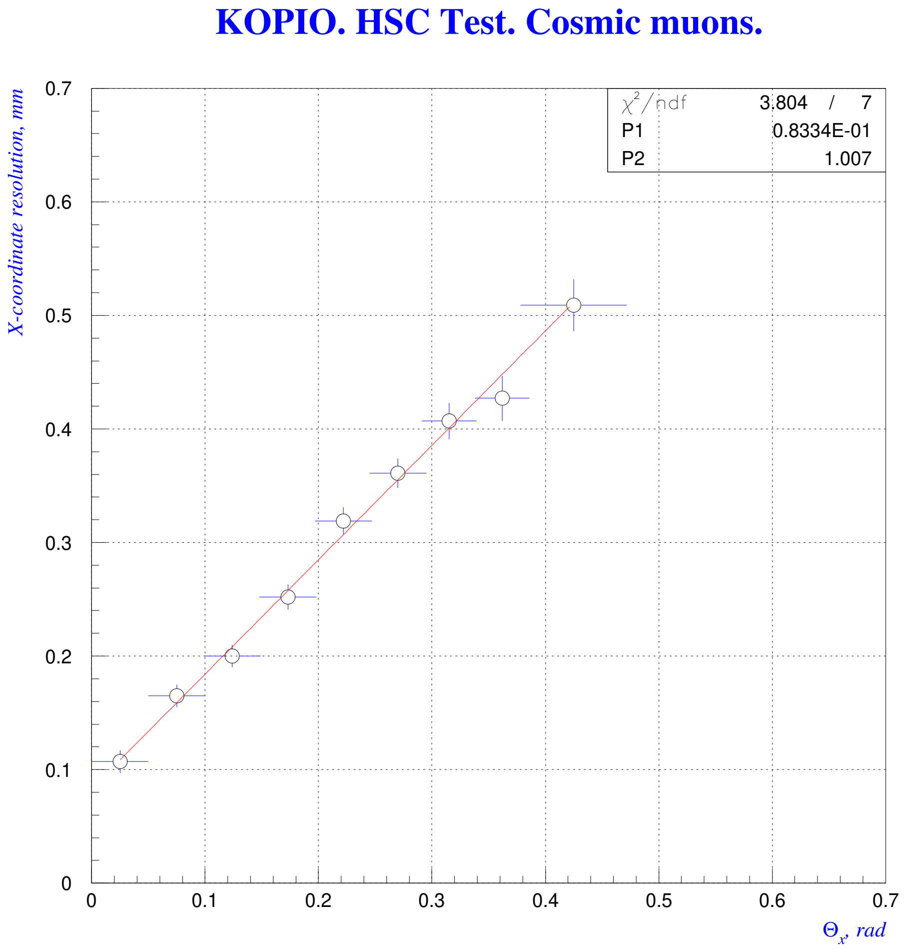

Figure 15: The spatial resolution of the strip readout versus the θ_x angle of cosmic ray muon incidence. The solid line is the the result of a linear fit. Extrapolated resolution from the fit is $\sigma_x = 83\ \mu m$ at $\theta_x = 0°$.

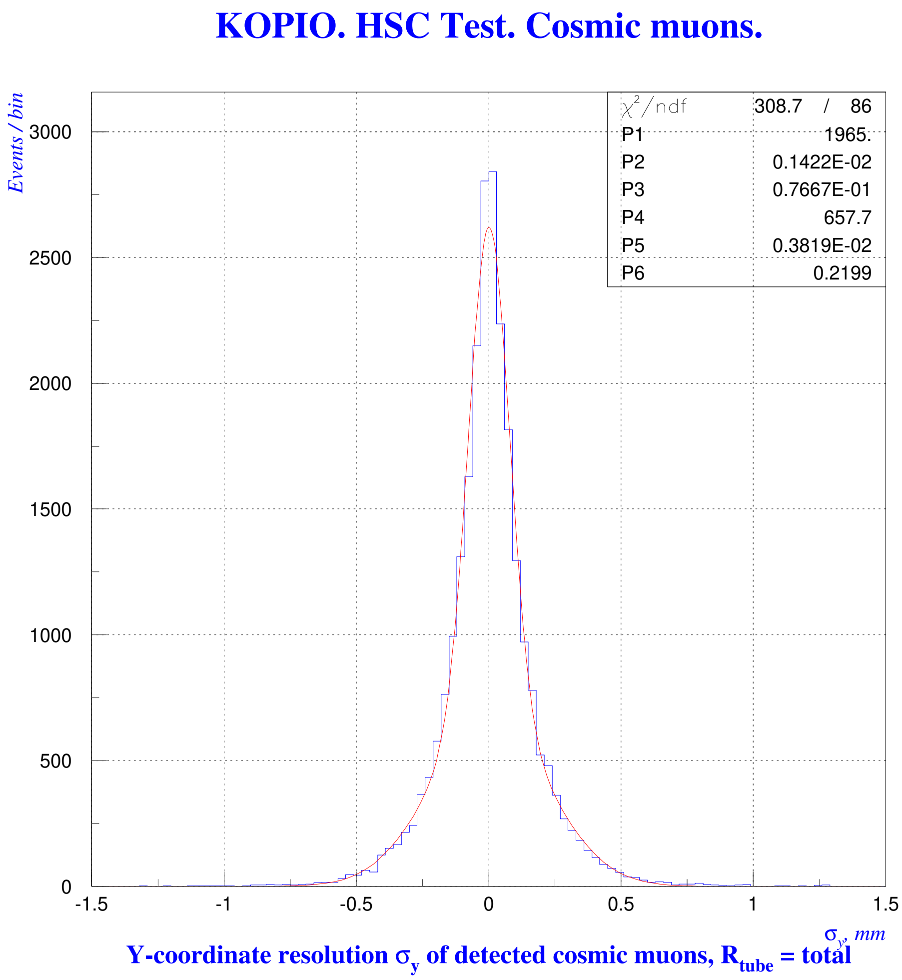

Figure 16: The measured residual resolution of wire readout planes for the total angular range of the detected cosmic ray muons. The solid curve is the sum of a two Gaussian fit with $\sigma_y = 77$ μm and 220 μm.

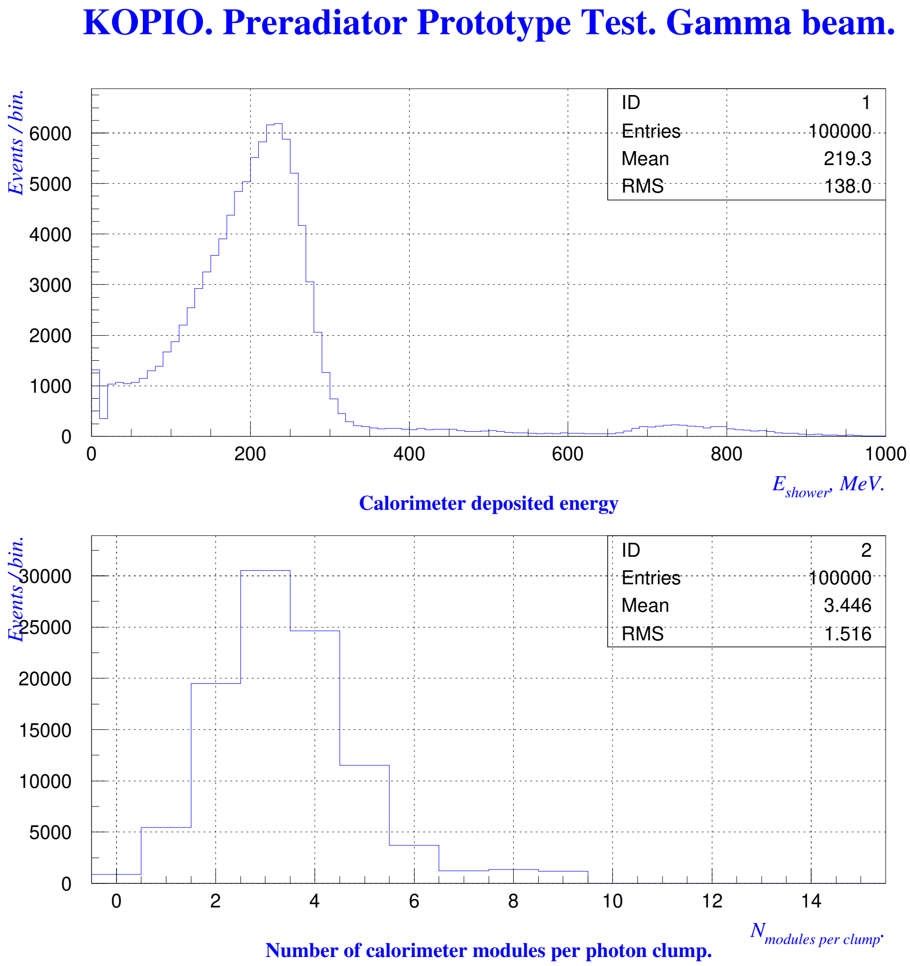

Figure 17: The measured energy distribution of the photon beam (upper histogram) using the nonet of Shashlik calorimeter modules. The lower histogram is the measured distribution of the number of calorimeter modules per photon clump.

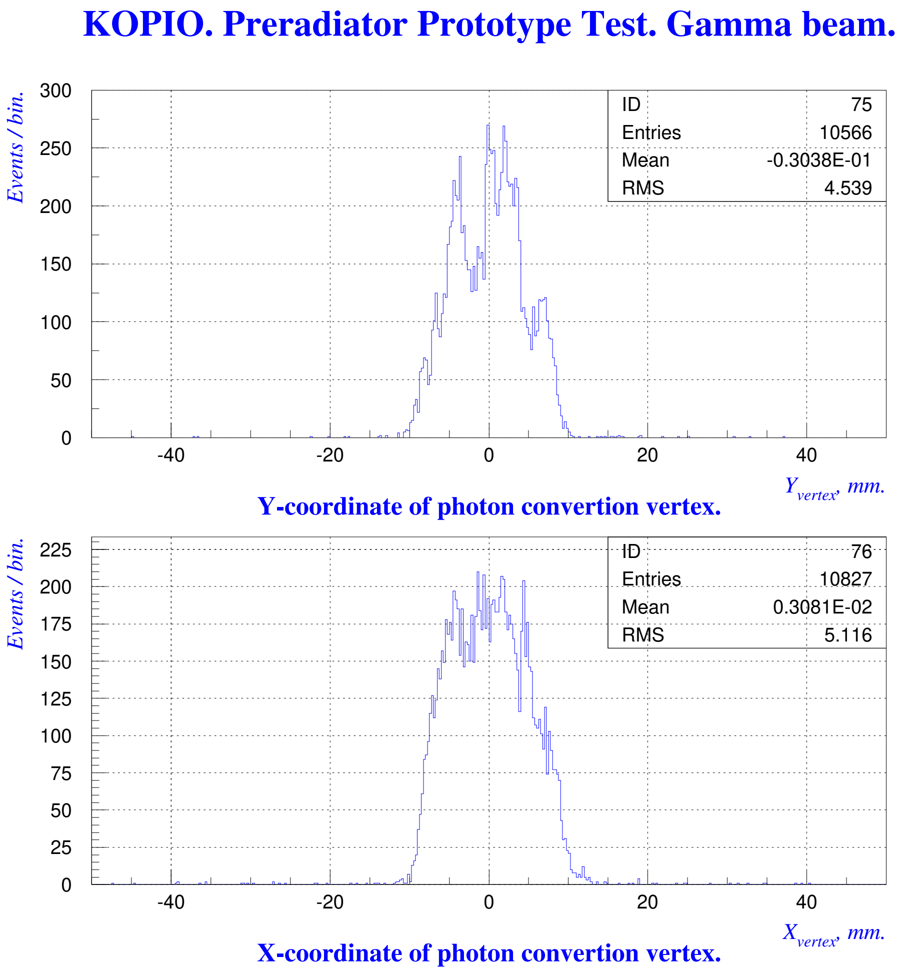

Figure 18: The vertical and horizontal position distributions of the photon conversion vertex for the photons converting in the second layer of chambers. The X- and Y- axes are perpendicular to beam line. The vertical and horizontal angles of incidence of the photon beam are $\sim 0°$, *i.e.*, perpendicular to the detector planes. The upper histogram is vertex position distribution for the wire readout. The lower histogram is vertex position distribution for strip readout.

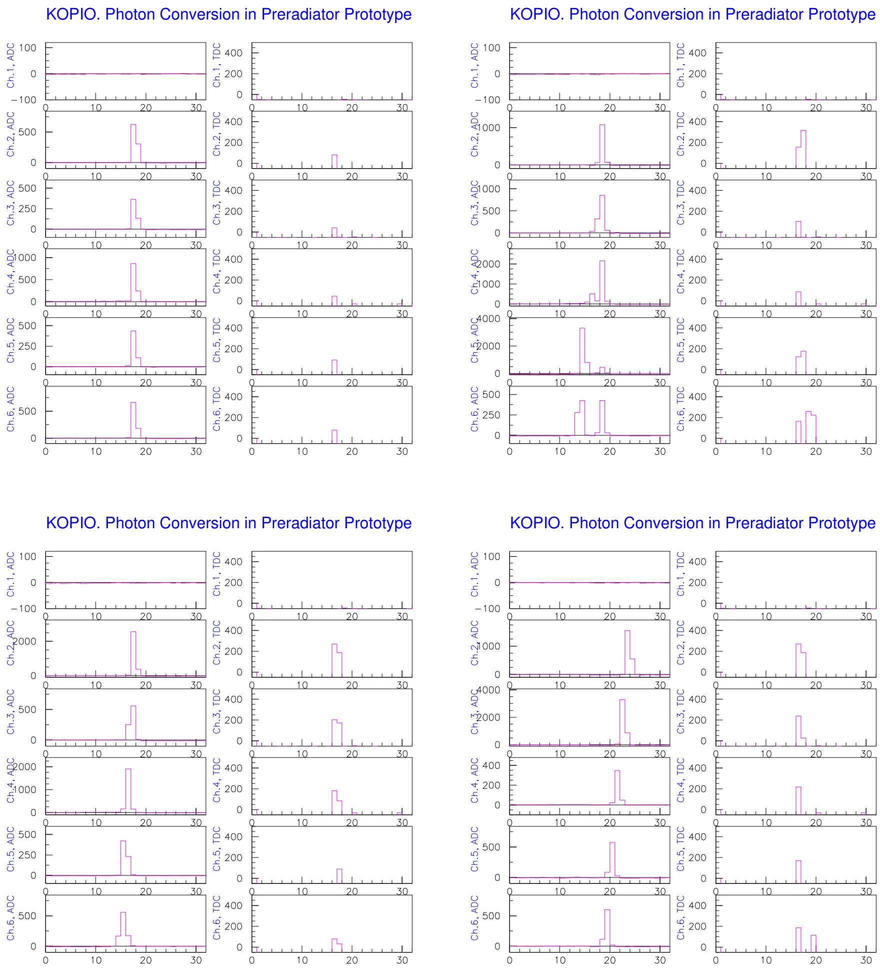

Figure 19: Examples of hits for photons in the preradiator. For each group of histograms the column is plane number (top being the first plane), and the rows are strip and wire readout, respectively. The upper histograms are events at $\theta \simeq 0°$. The lower histograms are events at $\theta \simeq 15°$ (left) and $\theta \simeq 30°$ (right). $\phi \simeq 0°$ in all cases.

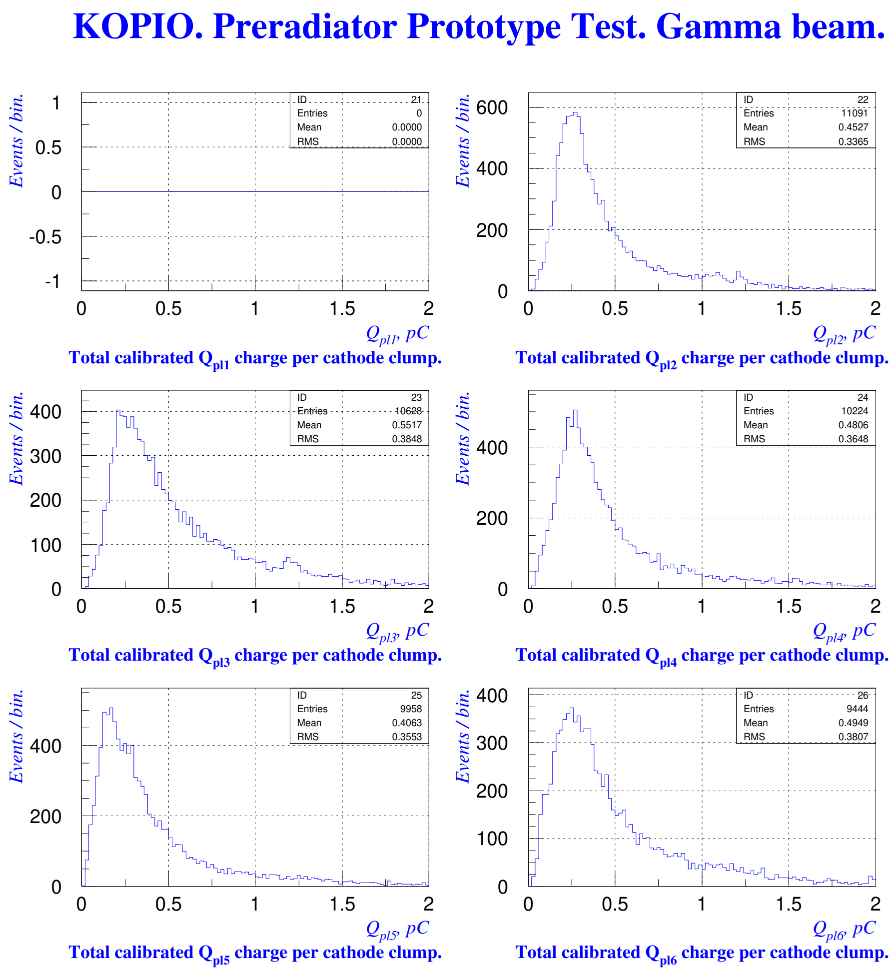

Figure 20: Collected charge distribution for photons.

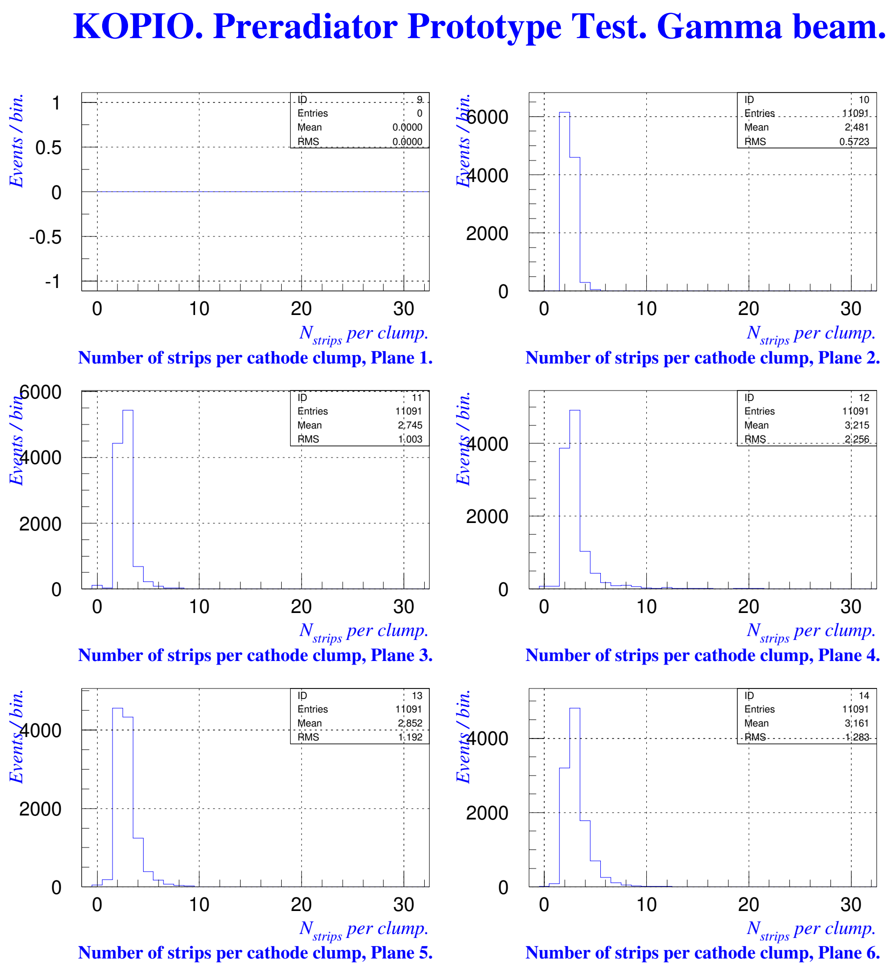

Figure 21: Distribution of the number of strips per plane per photon clump.

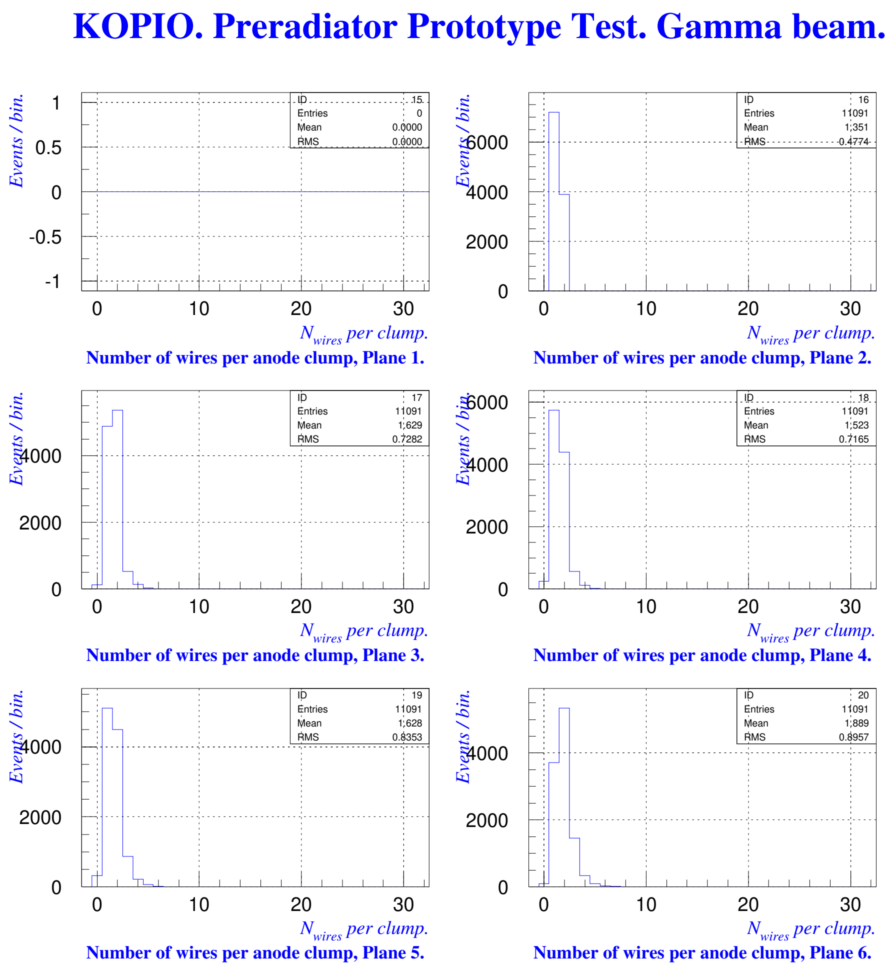

Figure 22: Distribution of the number of the wires per plane per photon clump.

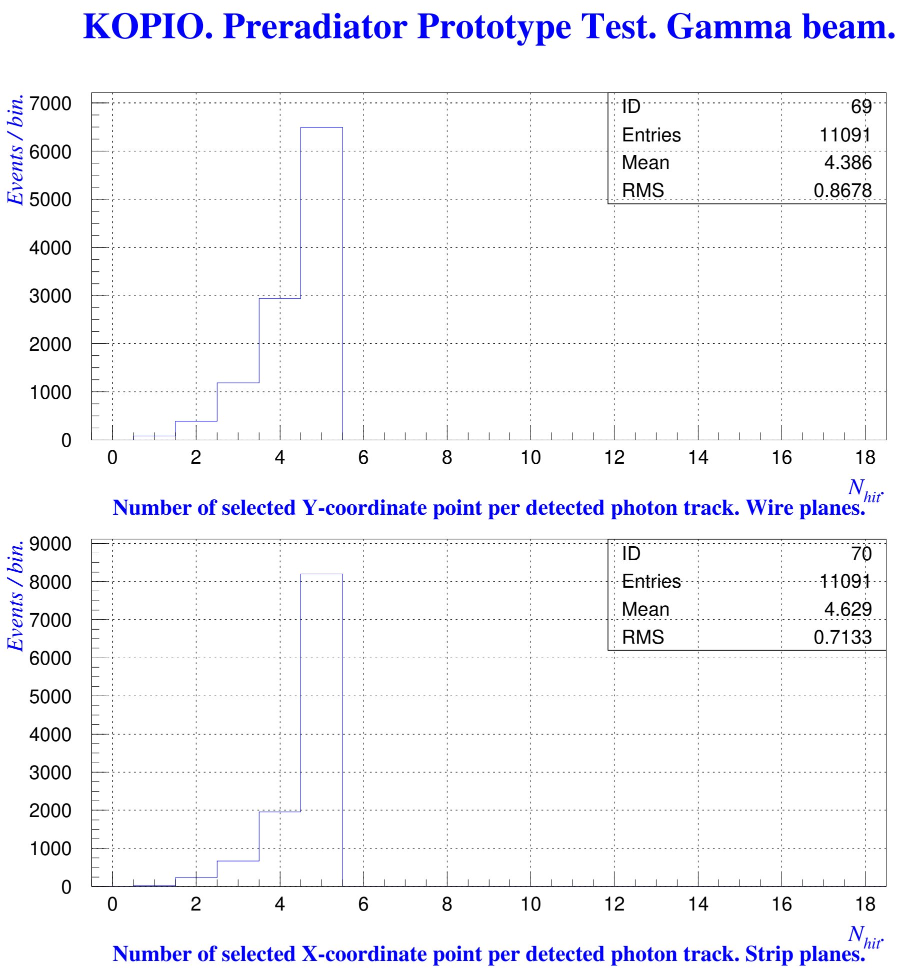

Figure 23: Distribution of number of planes with the “good” wire hits per reconstructed photon track (upper histogram). Distribution of number of planes with the “good” strip clumps per reconstructed photon track (lower histogram).

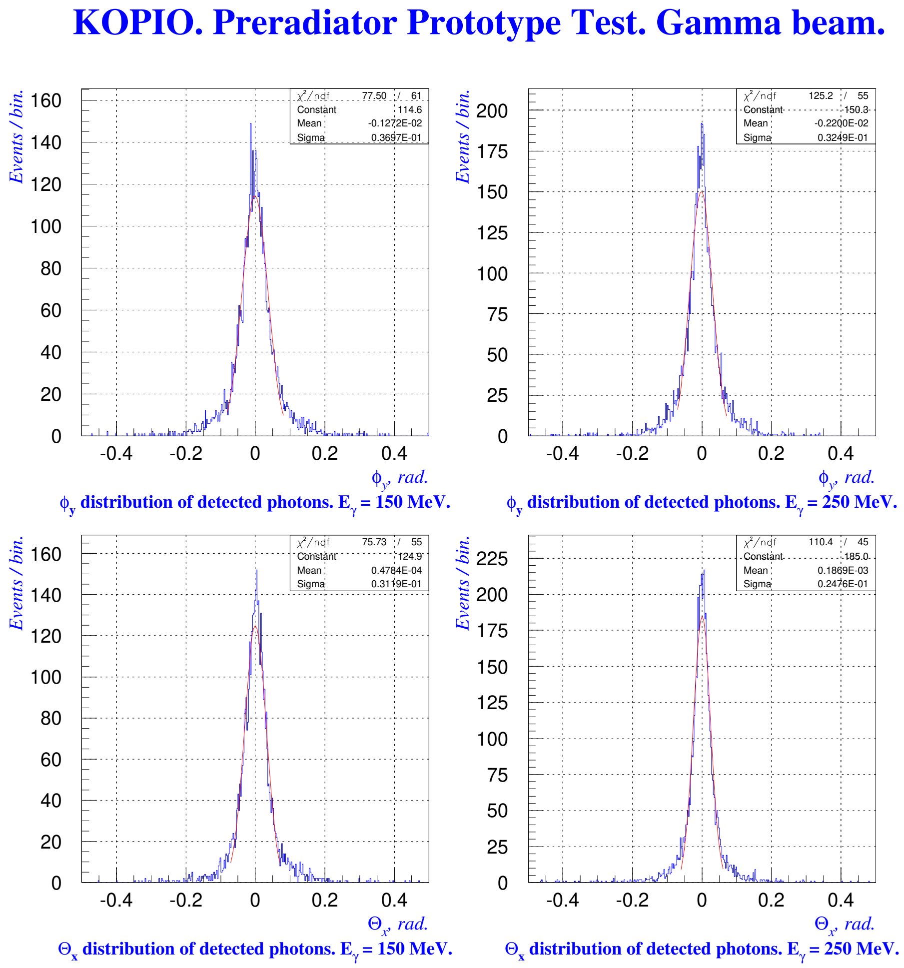

Figure 24: The measured angular distribution of photons for incident angle $\theta \simeq 0^\circ$ ($\phi \simeq 0^\circ$). The upper histogram for wire readout, the lower histogram is for strip readout. Left histograms are for photons in the energy range $100 \div 200$ MeV, right for $200 \div 300$ MeV.

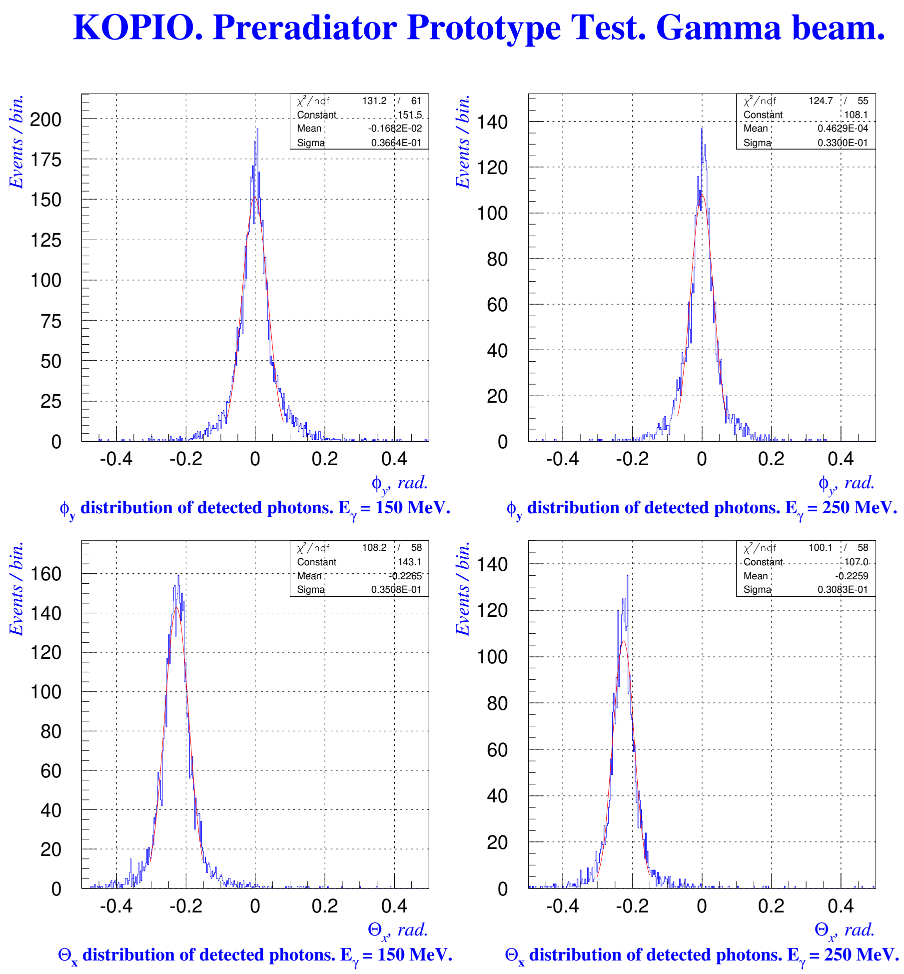

Figure 25: The measured angular distribution of photons for incident angle $\theta \simeq 15^\circ$ ($\phi \simeq 0^\circ$). The upper histogram for wire readout, the lower histogram is for strip readout. Left histograms for photon energy range $100 \div 200$ MeV, right for $200 \div 300$ MeV.

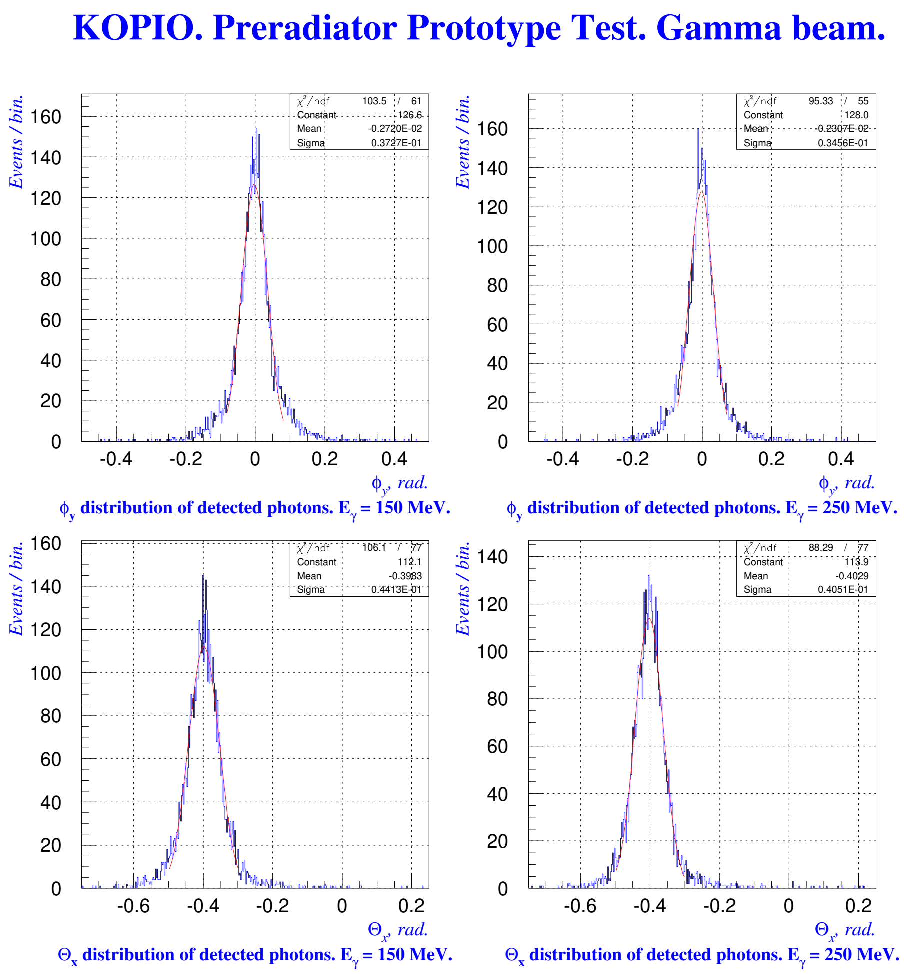

Figure 26: The measured angular distribution of photons for incident angle $\theta \simeq 30°$ ($\phi \simeq 0°$). The upper histogram for wire readout, the lower histogram is for strip readout. Left histograms for photon energy range $100 \div 200$ MeV, right for $200 \div 300$ MeV.